Low Temperature Physics/Fizika Nizkikh Temperatur, 2020, vol. 46, No. 12, pp. 1359–1364

Low-temperature studies of Cr^{3+} ions in natural and neutron-irradiated Mg-Al spinel

N. Mironova-Ulmane, A. I. Popov, G. Krieke, A. Antuzevics, V. Skvortsova, E. Elsts, and A. Sarakovskis

Institute of Solid State Physics, University of Latvia, Riga LV-1063, Latvia
E-mail: Nina.Mironova-Ulmane@cfi.lu.lv

Received September 3, 2020, published online October 21, 2020

Original results on the EPR and photoluminescence Cr^{3+} ions in natural magnesium aluminum spinel ($MgAl_2O_4$) are presented. The photoluminescence spectra of Cr^{3+} ions in natural $MgAl_2O_4$ have been measured before and after irradiated by fast neutrons.

Keywords: photoluminescence spectra, $MgAl_2O_4$, fast neutrons.

1. Introduction

Oxide materials with a spinel structure of the general formula AB_2O_4 (A = Mg, Zn; B = Al, Ga) demonstrate unique physicochemical properties, which determines their extensive research and growing interest in their use in various scientific and industrial applications [1–9]. Among all the metal oxides, magnesium aluminate spinel ($MgAl_2O_4$), receives specific attention [1–3, 10]. $MgAl_2O_4$ is a refractory oxide material with high toughness and chemical stability, low electrical conductivity, and low density (~ 3.6 g/cc), high melting temperature (~ 2150 °C), and it is transparent in the visible and infrared wavelength regions. Their attractive optical and luminescent properties, high thermal and chemical stability, as well as high resistance to radiation damage, make these compounds suitable for a very wide range of different applications, including electroluminescent and vacuum fluorescent displays, light-emitting diodes, solid-state lasers, UV photodetectors, as well as optically-stimulated storage and long persistent phosphors, IR windows as well as functional optical and dielectric materials for nuclear fusion reactor applications [9–23]. Ceramic $MgAl_2O_4$ materials are also planned to be exploited as a porous material for different sensor applications, such as humidity control [24–27].

Spinel compound $MgAl_2O_4$ belongs to the space group $Fd\bar{3}m$ No. 227 in the International Tables. Consequently, there are $Z = 8$ formula units per cubic unit cell, each of which consists of 32 anions and 24 cations, for a total of 56 atoms. The Bravais lattice of the conventional unit cell is face-centered cubic (fcc); the basis consists of two formula units. In the normal structure of spinel, eight the Mg^{2+} cations occupy tetrahedrally coordinated *A*-positions with T_d symmetry and 16 of the Al^{3+} cations occupy octahedrally coordinated *B*-positions with D_{3d} symmetry, respectively. In the inversion structure of $MgAl_2O_4$, eight of the Al^{3+} ions occupy tetrahedrally coordinated *A*-positions, and eight of the Mg^{2+} ions and eight of the Al^{3+} ions occupy octahedrally coordinated *B*-positions.

Historically, the word spinel originated as the magnesium/aluminum member of the larger spinel group of minerals. Natural spinels $MgAl_2O_4$ have an almost normal cationic order, while synthetic spinels exhibit significant inversion. Natural samples of spinel $MgAl_2O_4$ almost always contain Cr^{3+} impurities, which isomorphically substitute for Al^{3+} ions. The presence of such chromium ions gives the effect of the appearance of red color, the tonality of which depends on the concentration of chromium. The luminescent properties of Cr and Mn in $MgAl_2O_4$ and related compounds with a spinel structure have been intensively studied over the past several decades [28–31]. Note, that corresponding detailed studies of the structure and phase transformations in natural and synthetic crystals of magnesium-aluminum spinel containing transition metal ions (Cr^{3+}, Mn^{2+}) were carried out after irradiation with fast neutrons [32, 33]. In addition, using EPR, optical absorption, and cathodoluminescence, intrinsic structural radiation defects and their thermal annealing in stoichiometric $MgAl_2O_4$ single crystals and nonstoichiometric $MgO{\cdot}2.5Al_2O_3$ irradiated with fast neutrons have been studied in detail [10, 13, 14, 34–36].

In this work, we present original results on the photoluminescence Cr^{3+} ions in natural magnesium aluminum spinel before and after irradiated by fast neutron.

2. Experimental

The natural spinel samples used in the present investigation are a pink specimen from Ural and Pamir mountain

deposits. The amount of Cr^{3+} impurity in spinel samples was determined using instrumental neutron activation analysis techniques [37]. The neutron irradiation was performed in the Latvian 5MW water-water research reactor.

The fluence of fast neutrons with energy more than 0.1 MeV was in the range of 10^{14} n/cm^2. As for the irradiation temperature, it was 293 K. A cadmium filter was used for thermal neutron absorption. EPR spectra in the range of 5–40 K were measured on a CW-EPR Bruker ELEXSYS-II E500 spectrometer equipped with a flow-through cryostat with liquid helium. The modulation parameters of the magnetic field were 100 kHz and 4 G; microwaves were generated at a frequency of 9.36 GHz and a power of 0.2 mW.

Luminescence spectra were measured with an Ekspla NT342/3UV tunable pulsed solid-state laser. The luminescence was recorded by an Andor iStar DH734 CCD camera coupled to the Andor SR-303i-B spectrometer, equipped with grating of 600 lines/mm (resolution 1 nm) and 2400 lines/mm (resolution 0.1 nm) using CCD camera. Low temperature measurements were performed using Advanced Research Systems DE202 N cold finger type He cryostat.

3. Results

3.1. EPR spectroscopy

The low-temperature EPR spectra of a natural spinel sample measured at several temperatures for the chosen orientation are shown in Fig. 1. The inset to Fig. 1 shows the details of the spectrum in the range of fields 3000–4000 G, recorded at 5 K (lower curve) and 10 K (upper curve), respectively.

The EPR spectra contain several high-intensity resonances in the 1000–3000 G range as well as weaker lines in the vicinity of $g = 2$. A decrease in temperature leads to an increase in the intensity of the EPR signal, which, due to the Boltzmann distribution, is associated with a large difference in the population of spin levels until the effects of power saturation appear [38, 39]. The high-intensity signal is associated with chromium impurities, which are almost always present in such samples. At the microwave *X*-band frequency, Cr^{3+} in $MgAl_2O_4$ spinel represents a case where the zero-field splitting (ZFS) is much larger than the Zeeman term. As a result, EPR transitions occur in the range $g \approx 4$–2 regardless of the exact value of ZFS [40].

It is known that Cr^{3+} in $MgAl_2O_4$ forms axial and orthorhombic centers and complexes of Cr^{3+}–Cr^{3+} ion pair [41–45]. In the spectra of Fig. 1, the dominant contribution is made by the axial center, which is formed by the replacement of Cr^{3+} for the Al^{3+} sites in the spinel structure.

The intensity of the Cr^{3+} EPR signal follows the $1/T$ dependence for the chosen microwave power, while the resonance linewidth remains practically unchanged. The fact that the linewidth is independent of temperature means that spin-spin interactions play a dominant role in relaxation processes [46]. In addition, overlapping signal patterns are observed in the 3000–4000 G field range. The six-component structure is a characteristic feature of Mn^{2+} impurities and can be explained by the interaction of the electron spin system with the ^{55}Mn nuclear spin $I = 5/2$. The average distance between the lines is ≈ 82 G, which is comparable to the value of 83 G determined for Mn-doped synthetic spinel [47]. The decrease in the intensity of the Mn^{2+} signal with temperature does not occur as fast as for Cr^{3+}. Comparison of the intensity of the EPR signals of Cr^{3+} and Mn^{2+} as a function of temperature is shown in Fig. 2, where the curves are normalized to the amplitude of the signal detected at 40 K.

Comparison of the spectra in the inset to Fig. 1 that there is an additional resonance at $g = 1.98$. Based on the value of g, the signal can be associated with Ti^{3+} impurities present in the sample [48]. Thus, by analysing the EPR signals

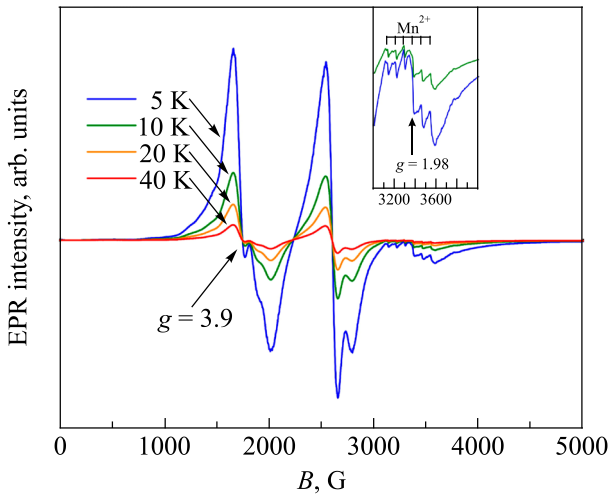

Fig. 1. (Color online) EPR spectra of the natural spinel sample for the chosen orientation in 5–40 K temperature range. The inset represents a spectra details in the range of 3000–4000 G spectral region at 5 K (lower curve) and 10 K (upper curve).

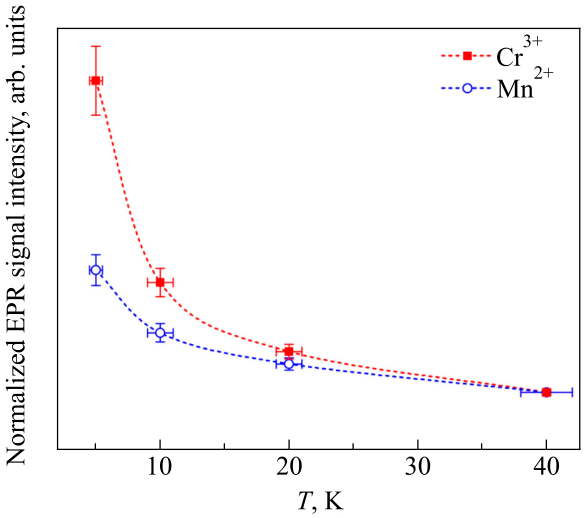

Fig. 2. (Color online) Dependence of the Cr^{3+} and Mn^{2+} EPR signal intensity as a function of temperature. Curves have been normalized for signal intensities at 40 K.

at a variable temperature and based on the differences in the temperature characteristics of the EPR signal, one can successfully identify the existing impurities in the samples.

3.2. Photoluminescence spectra

Natural crystals of magnesium-aluminum spinels almost always contain an uncontrolled admixture of chromium. It is known that the stabilization energy of chromium ions in the octahedral position is much higher than the stabilization energy in the tetrahedral position. In particular, according to [49], the corresponding so-called octahedral site preference energy (OSPE) of Cr^{3+} in $MgAl_2O_4$ crystal structures is 37.5 kcal/mol. The OSPE parameter is the difference between the crystal field energy of a cation in octahedral coordination (CFSEo) and that in tetrahedral coordination (CFSEt).

Therefore, the chromium ions in the crystal structure of the spinel always occupy octahedral positions. In this position local symmetry of its environment sites is the D_{3d} point symmetry. It should be noted the photoluminescence spectra of zero-phonon lines of Cr^{3+} ions (*R*-lines, *N*-lines) and their phonon sidebands (*R*-PSB, *N*-PSB) were previously observed in [50, 51], as a comparative analysis of the effect of neutron irradiation has not yet been investigated. Figure 3 shows the luminescence spectra of natural lilac $MgAl_2O_4$ (Cr^{3+} mass concentration $9.8\cdot10^{-5}$ %) in the range of the doublet zero-phonon *R*-lines, measured from 10 K up to 300 K with the step of 10 K.

Photoluminescence spectra of Cr^{3+} centers in $MgAl_2O_4$ obtained at $\lambda_{ex} = 550$ nm with resolution 0.1, have doublet zero-phonon *R*-lines: $R_1 = 684.4$ nm and $R_2 = 684.7$ nm at 10 K. It is also seen that the zero-phonon *R*-lines position shifts and its intensity decreases with increasing temperature. The corresponding photoluminescence spectra of Cr^{3+} ions of the natural spinel $MgAl_2O_4$ (lilac, concentration Cr $9.8\cdot10^{-5}$, mass %), excited with $\lambda_{exc} = 550$ nm through the $^4A_{2g} \rightarrow {}^4T_{2g}$ allowed transition at room temperature (RT) and 10 K are shown in Fig. 4, from which we can see efficient red emission in the region around 670–730 nm, due to the spin-forbidden transition $^2E_g \rightarrow {}^4A_{2g}$ of Cr^{3+} ions located at the sites with local symmetry D_{3d}. In Fig. 4, we can also see that all the luminescence lines are shifted towards high energies, and its half-width narrows, therefore the *N*-lines in the luminescence spectra appear at 10 K.

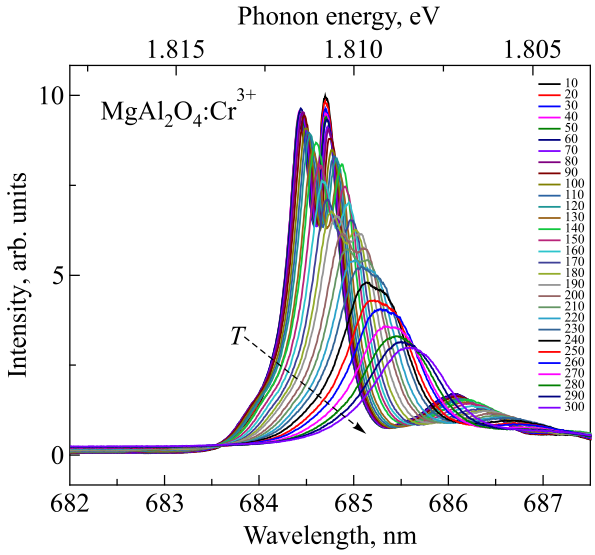

Fig. 3. (Color online) Temperature-dependent luminescence spectra of natural lilac $MgAl_2O_4$ (Cr^{3+} mass concentration $9.8\cdot10^{-5}$ %) in the range of the doublet zero-phonon *R*-lines.

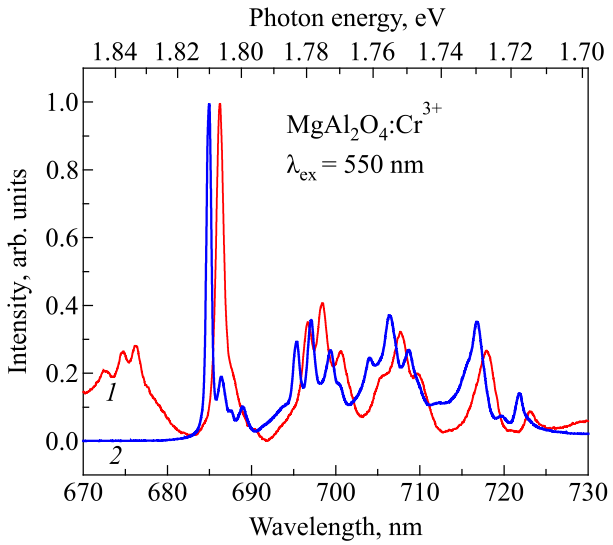

Fig. 4. (Color online) The photoluminescence spectra of natural lilac $MgAl_2O_4:Cr^{3+}$, excitation wavelength $\lambda_{ex} = 550$ nm, measurement temperatures: RT (red, *1*); 10 K (blue, *2*).

In addition to the *R*- and *N*-lines, caused by zero-phonon transitions, the photoluminescence spectra of Cr^{3+} at low temperatures exhibit broad electronic structures, located on the long-wavelength side from zero-phonon lines. Whereas at room temperature, a single-phonon vibronic sideband arises from the short and long-wavelength side of the zero-phonon *R*-line. Note that phonon-induced anti-Stokes photoluminescence of Cr^{3+} ions has already been observed under laser excitation in [52]. Note also that in [53] it was stated that the PL spectrum of Cr^{3+} in the ceramic spinel $ZnAl_2O_4$ consists of a zero-phonon (*R*) line as well as two symmetric sets of narrow lines at the long-wavelength and short-wavelength sides of the *R*-line, which were attributed to Stokes and anti-Stokes vibronic bands.

Figure 5 shows a normal environment (a) of the Cr^{3+} ion and one of the variants of replacement one Al^{3+} ion by an Mg^{2+} ion. As is already well known and accepted, *N*-lines are associated with chromium ions, the local symmetry of the environment of which depends on the symmetry of the environment of ions in the crystalline structure of normal spinel. Earlier Mikenda *et al.* [50, 51] studied in detail zero-phonon *N*-lines in the luminescence spectra of Cr^{3+}-doped spinels and showed that zero-phonon *N*-lines appear in the presence of inverse distribution of cations in spinel.

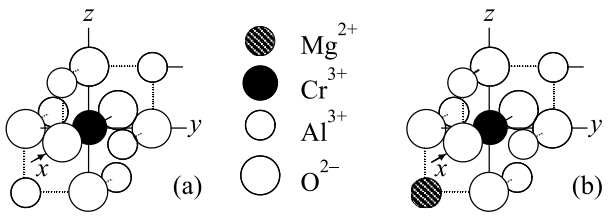

Fig. 5. Normal environment (a) of Cr^{3+} ion and one of the variants of the inverse environment, (b) of the Cr^{3+} ion in $MgAl_2O_4$.

Figure 6 shows the photoluminescence spectrum of natural dark pink $MgAl_2O_4:Cr^{3+}$ (mass concentration Cr^{3+} $8\cdot10^{-2}$ %) measured at 10 K, excitations wavelength $\lambda_{ex} = 550$ nm. The observed photoluminescence spectrum, which is excited at the spin-allowed transitions ${}^4A_{2g} \rightarrow {}^4T_{2g}$ (550 nm), consists of a zero-phonon *R*-line and two zero-phonon *N*-lines. It can be seen that the intensity of these three lines is practically the same. Note that other low-intensity zero-phonon *N*-lines are also observed, which overlap with the one-phonon vibronic sideband.

The following Fig. 7 shows the photoluminescence spectra of natural lilac $MgAl_2O_4:Cr^{3+}$, irradiated with a fast neutron fluence of 10^{14} n/cm^2 and measured at 10 K, using several excitation wavelengths: (350 nm; 540 nm; 595 nm). In this case, the excitation of various electronic transitions was used to see the specific structure of the photoluminescence spectra of $MgAl_2O_4$. Thus, the photoluminescence of Cr^{3+} ions in neutron-irradiated natural (lilac) $MgAl_2O_4$ was excited via spin-allowed transitions ${}^4A_{2g} \rightarrow {}^4T_{1g}$, (350 nm), ${}^4A_{2g} \rightarrow {}^4T_{2g}$, (550 nm) and nearby located sharp lines of spin-forbidden transitions from the ground state ${}^4A_{2g}$ to the excited states ${}^2E_g$. Finally, the last Fig. 8 shows the photoluminescence spectra of natural dark pink $MgAl_2O_4:Cr^{3+}$

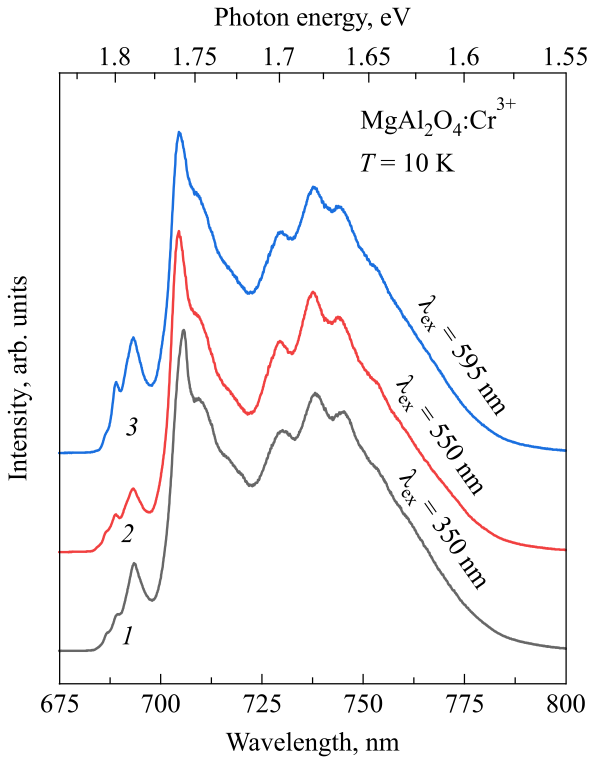

Fig. 7. The photoluminescence spectra of natural lilac $MgAl_2O_4:Cr^{3+}$ irradiated with fast neutron fluence 10^{14} n/cm^2, measured at 10 K, excitation wavelengths λ_{ex}, nm: 350 (*1*), 540 (*2*), 595 (*3*).

irradiated with fast neutron fluence 10^{14} n/cm^2 and measured at 10 K under excitation in spin-allowed transitions ${}^4A_{2g} \rightarrow {}^4T_{1g}$, (350 nm), ${}^4A_{2g} \rightarrow {}^4T_{2g}$, (550 nm).

In Table 1, we summarized the most important characteristics of the samples that were investigated in this work, namely, the concentration of chromium impurities in Lilac

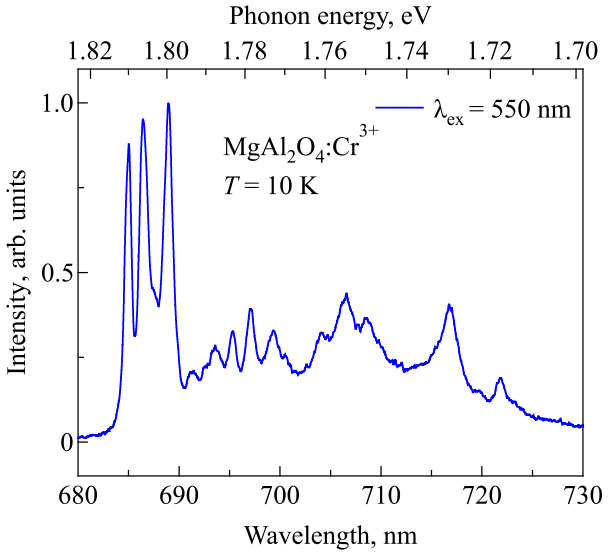

Fig. 6. The photoluminescence spectrum of natural dark pink $MgAl_2O_4:Cr^{3+}$ (mass concentration Cr^{3+} $8\cdot10^{-2}$ %) measured at 10 K, excitations wavelength $\lambda_{ex} = 550$ nm.

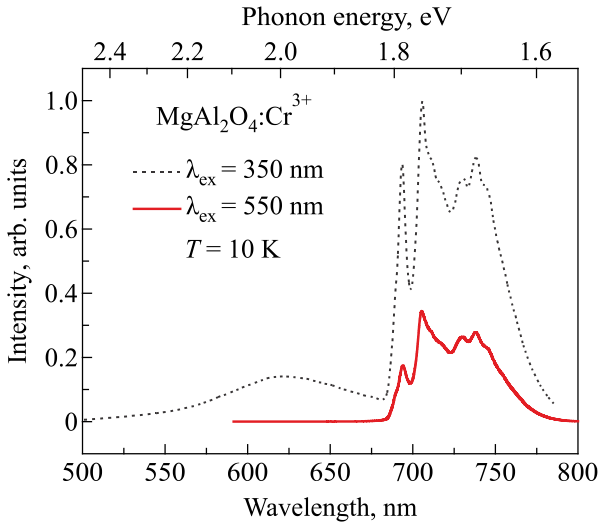

Fig. 8. The photoluminescence spectra measured at 10 K of natural dark pink $MgAl_2O_4:Cr^{3+}$ irradiated with fast neutron fluence 10^{14} n/cm^2.

Table 1. Luminescent characteristics of natural $MgAl_2O_4$ (lilac and dark pink) before and after irradiation

		$MgAl_2O_4$: Cr^{3+}						
Cr^{3+} concentration, mass %		Lilac				Dark pink		
		$9.8\cdot10^{-5}$				$8\cdot10^{-2}$		
Neutron fluence D, n/cm^2		Virgin	10^{14}			Virgin	10^{14}	
λ_{ex}, nm		550	350	550	595	550	350	550
Temperature, K		10	10	10	10	10	10	10
Emission peaks, nm	R	685.0	–	–	–	685.0	–	–
	N_1	686.3	–	–	–	686.3	–	–
	N_2	687.6	–	–	–	–	–	–
	N_3	688.9	689.2	689	689	688.9	–	–
	N_4	–	693.4	693.2	693.2	–	692.8	692.8
	N_5	–	705.7	704.5	704.6	–	704.6	704
Figure		Fig. 4	Fig. 7			Fig. 6	Fig. 8	

and Dark Pink $MgAl_2O_4$ samples, the neutron fluencies to which the samples were exposed, the excitation wavelengths for luminescence measurements, the peaks of the obtained spectra, the attribution of these peaks, as well as the numbering of figures in which the spectra are shown. All measurements were carried out at 10 K.

4. Conclusion

The photoluminescence spectra Cr^{3+} in the natural $MgAl_2O_4$ spinel consist of zero-phonon R- and N-lines due to the $^2E_g \rightarrow {}^4A_{2g}$ spin-forbidden transition and their Stokes and anti-Stokes one-phonon vibronic sidebands.

The doublet zero-phonon R-lines: $R_1 = 684.4$ and $R_2 = 684.7$ nm was observed at 10 K and resolution 0.1 nm.

We have observed that the intensity of zero-phonon N-lines for two natural spinels depends on the chromium concentration.

After irradiation with fast neutrons, the photoluminescence spectra Cr^{3+} in the natural spinel $MgAl_2O_4$ no longer show zero-phonon R-line, zero-phonon N_1–N_2 lines and at a high chromium concentration, zero-phonon N_3 also disappeared.

The predominant contribution to the EPR spectra is made by the axial centre, which is formed by the substitution of Cr^{3+} for Al^{3+} sites in the spinel structure.

EPR analysis at variable temperature allows the identification of impurities in naturally occurring samples based on differences in the temperature characteristics of the EPR signal.

Acknowledgements

This study was supported by a grant from Latvian Council of Science (agreement No. LZP-2018/1-0214).

1. I. Ganesh, *Int. Mater. Rev.* **58**, 63 (2013).
2. M. R. Merac, H. J. Kleebe, M. M. Müller, and I. E. Reimanis, *J. Am. Ceram. Soc.* **96**, 3341 (2013).
3. A. Goldsteing, *J. Eur. Ceram. Soc.* **32**, 2869 (2012).
4. A. Maleki, Z. Hajizadeh, and P. Salehi, *Sci. Rep.* **9**, 5552 (2019).
5. S. Sharifi, A. Yazdani, and K. Rahimi, *Sci. Rep.* **10**, 10916 (2020).
6. D.-W. Kim, S. Uchida, H. Shiiba, N. Zettsu, and K. Teshima, *Sci. Rep.* **8**, 11771 (2018).
7. F. Caddeo, D. Loche, M. F. Casula, and A. Corrias, *Sci. Rep.* **8**, 797 (2018).
8. C.-L. Yeh and Y.-C. Chen, *Crystals* **10**, 210 (2020).
9. A. Luchechko, Y. Zhydachevskyy, S. Ubizskii, O. Kravets, A. I. Popov, Y. Rogulis, E. Elsts, E. Bulur, and A. Suchocki, *Sci. Rep.* **9**, 9544 (2019).
10. A. Lushchik, E. Feldbach, E. A. Kotomin, I. Kudryavtseva, V. N. Kuzovkov, A. I. Popov, V. Seeman, and E. Shablonin, *Sci. Rep.* **10**, 7810 (2020).
11. A. Jouini, A. Yoshikawa, A. Brenier, T. Fukuda, and G. Boulon, *Phys. Status Solidi C* **4**, 1380 (2007).
12. E. M. Yoshimura and E. G. Yukihara, *Radiat. Meas.* **41**, 163 (2006).
13. A. Platonenko, D. Gryaznov, Yu. F. Zhukovskii, and E. A. Kotomin, *Phys. Status Solidi B* **255**, 1800282 (2018).
14. V. T. Gritsyna, Y. G. Kazarinov, V. A. Kobyakov, and K. E. Sickafus, *Rad. Eff. Def. Solids* **157**, 659 (2002).

15. T. Katsumata, H. Takeuchi, S. Komuro, and H. Aizawa, *Rev. Sci. Instrum.* **89**, 095104 (2018).
16. V. T. Gritsyna, Yu. G. Kazarinov, A. O. Moskvitin, and I. E. Reimanis, *Acta Phys. Polon. A* **117**, 161 (2010).
17. S. P. Gokov, V. T. Gritsyna, V. I. Kasilov, S. S. Kochetov, and Y. G. Kazarinov, *Probl. Atom. Sci. Techn.* **5**, 81 (2009).
18. N. M. Khaidukov, M. N. Brekhovskikh, N. Yu. Kirikova, V. A. Kondratyuk, and V. N. Makhov, *Ceram. Int.* **46**, 21351 (2020).
19. E. F. Polisadova, V. A. Vaganov, S. A. Stepanov, V. D. Paygin, O. L. Khasanov, E. S. Dvilis, D. T. Valiev, and R. G. Kalinin, *J. Appl. Spect.* **85**, 416 (2018).
20. E. F. Polisadova, V. A. Vaganov, D. T. Valiev, S. A. Stepanov, V. D. Paygin, E. S. Dvilis, and O. L. Khasanov, *Phys. Solid State* **61**,1829 (2019).
21. D. Valiev, O. Khasanov, E. Dvilis, S. Stepanov, E. Polisadova, and V. Paygin, *Ceram. Int.* **44**, 20768 (2018).
22. D. Valiev, S. Stepanov, O. Khasanov, E. Dvilis, E. Polisadova, and V. Paygin, *Opt. Mater.* **91**, 396 (2019).
23. A. Luchechko, Y. Shpotyuk, O. Kravets, O. Zaremba, K. Szmuc, J. Cebulski, A. Ingram, R. Golovvchak, and O. Shpotyuk, *J. Adv. Ceram.* **9**, 432 (2020)
24. H. Klym, A. Ingram, O. Shpotyuk, J. Filipecki, and I. Hadzaman, *Phys. Status Solidi C* **4**, 715 (2007).
25. H. Klym, A. Ingram, O. Shpotyuk, I. Hadzaman, and V. Solntsev, *Nanoscale Res. Lett.* **11**, 133 (2016).
26. H. Klym, I. Hadzaman, and O. Shpotyuk, *Medziagotyra* **21**, 92 (2015).
27. H. Klym, A. Ingram, I. Hadzaman, I. Karbovnyk, I. Vasylchyshyn, and A. I. Popov, *IOP Conf. Ser.: Mater. Sci. Eng.* **503**, 012019 (2019).
28. N. Mironova, V. Skvortsova, A. Smirnovs, and L. Cugunov, *Opt. Mater.* **6**, 225 (1996).
29. T.-L. Phan, M.-H. Phan, and S.-C. Yu, *Phys. Status Solidi B* **241**, 434 (2004).
30. T.-L. Phan, S.-C. Yu, M.-H. Phan, and T. P. J. Han, *J. Korean Phys. Soc.* **45**, 63 (2004).
31. M. G. Brik, J. Papan, D. J. Jovanović, and M. D. Dramićanin, *J. Lumin.* **177**, 145 (2016).
32. N. Mironova-Ulmane, V. Skvortsova, A. Pavlenko, E. Feldbach, A. Lushchik, Ch. Lushchik, V. Churmanov, D. Ivanov, V. Ivanov, and E. Aleksanyan, *Rad. Meas.* **90**, 122 (2016).
33. V. Skvortsova, N. Mironova-Ulmane, and U. Ulmanis, *Nucl. Instr. Meth. B* **191**, 256 (2002).
34. V. Seeman, E. Feldbach, T. Kärner, A. Maaroos, N. Mironova-Ulmane, A. I. Popov, E. Shablonin, E. Vasil'chenko, and A. Lushchik, *Opt. Mater.* **91**, 42 (2019).
35. G. Prieditis, E. Feldbach, I. Kudryavstseva, A. I. Popov, E. Shablonin, and A. Lushchik, *IOP Conf. Ser.: Mater. Sci. Eng.* **503**,012021 (2019).
36. A. Lushchik, S. Dolgov, E. Feldbach, R. Pareja, A. I. Popov, E. Shablonin, and V. Seeman, *Nucl. Instr. Meth. B* **435**, 31 (2018).
37. D. Riekstina, O. Veveris, and V. Skvortsova, *J. Radioanal. Nucl. Chem.* **298**, 1907 (2013).
38. G. R. Eaton, S. S. Eaton, D. P. Barr, R. T. Weber, *Quantitative EPR*, Springer (2010), Vol. XII.
39. A. Abragam and B. Bleaney, *Electron Paramagnetic Resonance of Transition Ions*, in: *Electron Paramagn. Reson. Transit. Ions*, Oxford Clarendon press (1970), Vol. XIV.
40. J. Telser, *EMagRes.* **6**, 207 (2017).
41. R. Stahl-Brada and W. Low, *Phys. Rev.* **116**, 561 (1959).
42. S. B. Berger, *J. Appl. Phys.* **36**, 1048 (1965).
43. H. Van den Boom and J. C. M. Henning, *J. Phys. Chem. Solids* **34**, 1211 (1973).
44. J. C. M. Henning and H. Van Den Boom, *Phys. Rev. B* **8**, 2255 (1973).
45. D. Bravo and R. Böttcher, *Phys. Status Solidi* **170**, K109 (1992).
46. S. A. Al'tshuler and B. M. Kozyrev, *Electron Paramagnetic Resonance in Compounds of Transition Elements*, Wiley, 382 (1974).
47. J. S. Shaffer, H. A. Farach, and C. P. Poole, *Phys. Rev. B* **13**, 1869 (1976).
48. P. Lombard, B. Boizot, N. Ollier, A. Jouini, and A. Yoshikawa, *J. Cryst. Growth.* **311**, 899 (2009).
49. V. D'Ippolito, *Linking Crystal Chemistry and Physical Properties of Natural and Synthetic Spinels*: *an UV-VIS-NIR and Raman Study*, PhD thesis, Sapienza Universita di Roma, Italy (2013).
50. W. Mikenda, *J. Lumin.* **26**, 85 (1981).
51. W. Mikenda and A. Preisinger, *J. Lumin.* **26**, 67 (1981).
52. S. P. Feofilov and A. B. Kulinkin, *Opt. Mater.* **94**, 231 (2019).
53. N. M. Khaidukov, M. N. Brekhovskikh, N. Yu. Kirikova, V. A. Kondratyuk, and V. N. Makhov, *Ceram. Int.* **46**, 21351 (2020).

Низькотемпературні дослідження іонів Cr^{3+} у природній та опроміненій нейтронами Mg-Al шпінелі

N. Mironova-Ulmane, A. I. Popov, G. Krieke, A. Antuzevics, V. Skvortsova, E. Elsts, A. Sarakovskis

Представлено оригінальні результати щодо ЕПР та фотолюмінесценції іонів Cr^{3+} у природній шпінелі $MgAl_2O_4$. Спектри фотолюмінесценції іонів Cr^{3+} у природній $MgAl_2O_4$ виміряно до та після опромінення швидкими нейтронами.

Ключові слова: спектри фотолюмінесценції, $MgAl_2O_4$, швидкі нейтрони.